

Research Article

Electrocatalysis of Palladium Nanoparticles on Rough Graphite Electrodes Towards Hydrogen Evolution Reaction

Martina Schwager^{*}, Constanze Eulenkamp, Jenni Richter

Department of Applied Sciences and Mechatronics, Munich University of Applied Sciences, Lothstr. 34, 80335, München, Germany
E-mail: martina.schwager@hm.edu

Received: 14 April 2025; Revised: 29 May 2025; Accepted: 6 June 2025

Abstract: The electrocatalytic performance of palladium nanoparticles (PdNPs) supported on rough graphite for the hydrogen evolution reaction (HER) was investigated. Chronopotentiometric deposition resulted in a homogeneous distribution of PdNPs across the substrate surface. Electrochemical analysis of electrodes with varying Pd loadings demonstrated that HER proceeds via the Volmer-Heyrovsky mechanism, with a loading of $43 \mu\text{g}/\text{cm}^2$ achieving notable catalytic performance. Impedance spectroscopy revealed that the experimental data are accurately described by a two-time-constant parallel equivalent circuit model. At this optimal loading, mass transfer resistance was markedly reduced, particularly at high overpotentials. Under these conditions, charge transfer resistance became the dominant factor influencing HER activity, highlighting the importance of loading-dependent kinetics in optimizing catalytic performance.

Keywords: palladium nanoparticle, hydrogen evolution reaction, graphite, acidic media electrocatalysis, Tafel analysis, fuel cells, electrochemical impedance modeling

1. Introduction

In the expansive domain of sustainable energy generation, hydrogen has emerged as a crucial chemical energy storage medium, particularly with regard to its application in fuel cells [1, 2]. This versatile element demonstrates significant potential to supplant fossil fuels, facilitating energy production that yields only heat and water vapor as byproducts, thereby substantially mitigating greenhouse gas emissions [3, 4]. The prominence of hydrogen in this context is primarily attributed to its high energy density, zero-emission profile, and abundant reserves, positioning it as a cleaner and more sustainable alternative to conventional energy sources [5-7].

Among different energy storage and conversion technologies, the electrochemical splitting of water using the electricity produced from renewable energy sources such as solar and wind power enables hydrogen production without carbon footprint [8, 9]. Realizing the potential of hydrogen as a sustainable energy carrier requires surmounting substantial hurdles in its production, particularly in the realm of renewable energy-driven electrochemical water electrolysis. A critical challenge in this pursuit is the considerable energy expenditure associated with the water splitting process [10, 11].

The hydrogen evolution reaction and oxygen evolution reaction, which constitute the two half-reactions of water electrolysis, are kinetically inhibited, resulting in slow product formation [12]. This kinetic limitation necessitates the

Copyright ©2025 Martina Schwager, et al.
DOI: <https://doi.org/10.37256/aecm.6220256995>
This is an open-access article distributed under a CC BY license
(Creative Commons Attribution 4.0 International License)
<https://creativecommons.org/licenses/by/4.0/>

application of a significant overpotential to facilitate faster electron transfer and overcome the high activation energy barrier associated with the formation of reaction intermediates on the electrode surface [13]. The activation energy represents a kinetic constraint that must be surpassed to initiate and sustain the electrochemical reactions. Consequently, the efficiency of this crucial chemical process is intrinsically linked to the magnitude of the required overpotential. In light of this relationship, catalysts play a pivotal role in optimizing the water splitting reaction by minimizing the energy input necessary for hydrogen production and accelerating the overall reaction kinetics [14, 15].

Noble metal-based nanomaterials have demonstrated superior electrocatalytic performance for the hydrogen evolution reaction due to their optimal hydrogen binding energy, excellent stability, and tunable electronic properties [16, 17]. However, the scarcity of these materials in nature and their consequent high cost present substantial economic challenges [18, 19]. This makes decreasing their usage in order to achieve cost-effective hydrogen production necessary and has led to supported nanoparticle catalysts with low loading while still preserving the electrocatalytic properties [20, 21].

Among noble metals, platinum (Pt) stands out as the most effective catalyst for the electrochemical production of hydrogen, exhibiting near-zero overpotential [22]. However, its scarcity as a natural resource poses significant challenges for widespread application [23]. In the quest for alternative catalysts, palladium has emerged as a promising substitute for Pt. Pd shares many similarities with Pt in terms of its catalytic properties, demonstrating remarkable capabilities in hydrogen evolution reactions [24].

Carbon-based materials, including carbon black, graphene, carbon nanotubes, and nanofibers, are frequently employed as substrates in electrocatalysis due to their excellent stability and conductivity [25-28]. The graphitic skeleton of these materials exhibits high electrical conductivity, which facilitates efficient charge transfer from the support to the catalyst surface [29]. Furthermore, surface studies have elucidated that the structural and electronic properties of these carbon supports significantly influence the spatial distribution and stability of metal species [5].

This study investigates the electrocatalytic properties of palladium nanoparticles deposited on rough graphite substrates, examining the impact of varying palladium loadings. The inherent surface roughness and structural defects of the graphite substrate are hypothesized to promote extensive dispersion of PdNPs across diverse morphological sites, facilitating a uniform distribution of the catalytic material [30]. This heterogeneous surface topology is expected to provide a multitude of anchoring sites for the PdNPs, potentially enhancing catalyst stability by mitigating nanoparticle agglomeration and detachment [31].

The electrocatalytic performance of these PdNP-modified graphite substrates is analyzed by combining microscopic and electrochemical direct current (DC) and alternating current (AC) techniques. Scanning electron microscopy (SEM) is utilized to examine the texture of the electrode substrates, with a particular focus on the localization and morphology of the deposited palladium. The catalytic performance for the HER is evaluated using linear sweep voltammetry in 0.5 M H₂SO₄, assessing the promotion of higher hydrogen formation rates at equivalent applied potentials. Further insights into the kinetic processes and their relationship with electrocatalysis are gained through Tafel analysis and electrochemical impedance spectroscopy (EIS). The EIS technique is well-suited for distinguishing electrochemical processes with different time constants, enabling detailed investigation of both charge-transfer kinetics at the electrode interface and mass transport phenomena involving electroactive species [32, 33]. Conducting impedance analysis as a function of palladium loading offers a promising approach to catalyst characterization. This methodology facilitates a deeper understanding of how variations in catalyst composition influence the underlying kinetic mechanisms at different overpotentials. By systematically relating palladium content to electrochemical performance, this strategy can provide useful insights for optimizing catalyst utilization and improving the efficiency of hydrogen evolution.

2. Experimental

2.1 Preparation of palladium decorated graphite electrodes

Palladium decorated graphite electrodes (Pd/C) were prepared using PdCl₂ (Merck, Germany) with the concentration 9.4×10^{-3} mol/l in an acidic solution with 0.14 mol/l HCl (Merck, Germany).

Before the deposition of Pd, the graphite substrates (Phywe, Germany) were treated in an ultrasonic bath of acetone for 5 minutes. The electrodeposition was performed chronopotentiostatically for 15, 30, 60, 90, 120, 210 and 360 s onto

the graphite substrates applying a constant current of -1 mA. This resulted in Pd coverages ranging from 5 to 122 $\mu\text{g}/\text{cm}^2$. To minimize hydrogen evolution during deposition, the applied potential was consistently kept above 0.1 V vs. reversible hydrogen electrode (RHE) [34]. Following the electrodeposition, the electrodes were gently rinsed with deionized water and allowed to dry under ambient conditions.

2.2 Electrochemical characterization methods

All the electrochemical measurements were carried out using a PalmSens4 (PalmSens, Netherlands) at room temperature and a three electrode electrochemical system. The counter electrode was a graphite plate as opposed to a conventional Pt electrode to avoid any Pt leaching in the acidic medium during the hydrogen evolution. An Ag/AgCl electrode in 3 M KCl was used as a reference electrode.

Linear sweep voltammetry (LSV) was performed in a 0.5 M H_2SO_4 electrolyte with a scan rate of 5 mV/s in the potential range from 0.01 V to -0.29 V vs. RHE. Prior to recording the polarization curves, cyclovoltamograms (CV) were taken (50 mV/s) until a stable current voltage curve over the potential range was obtained. The polarization curves were calibrated according to RHE using the equation $E_{\text{RHE}} = E_{\text{Ag/AgCl}} + 0.207 \text{ V} + 0.059 \text{ V} \cdot \text{pH}$. The 0.5 M sulfuric acid had a pH value of 0.48.

Electrochemical impedance spectroscopy was performed within a frequency range from 50 kHz to 0.02 Hz to cover at least partially various kinetic processes with corresponding time constants in the range of 3.2×10^{-6} s to 8 s. A sinusoidal AC voltage of 0.01 V was applied. The linearity of the measurements was tested with an AC signal of 5×10^{-3} V giving identical results. For selected electrodes DC potentials ranging from -10 to -65 mV vs. RHE were applied. The EIS data were taken varying the DC voltage from low to high overpotentials to ensure that the small current signals at low overpotentials were not disturbed by excessively adherent hydrogen bubbles formed due to the previously applied higher voltages. The real and imaginary parts of the EIS were normalized with respect to the geometric surface of the electrodes. The recorded impedance data were analyzed using the Zview circuit fitting software.

3. Results and discussion

3.1 Surface characterization

The morphology and structure of the nanoparticles and anchoring sites on the graphite substrate can provide significant influence on the catalytic HER performance [35]. The deposition characteristics of the palladium particles were studied using SEM for different prepared electrodes.

The mass m_{pd} of the deposited Pd is calculated according to Faradays law under consideration of 2 electrons needed for the reduction of Pd^{2+} . The metal loadings for the varying electrodes divided by the geometric area that was immersed in the palladium solution during the deposition process are listed in Table 1. Figure 1 depicts SEM micrographs taken from two electrodes with differing loadings to get insight into the deposition and growth process of the metal nanostructures.

Table 1. Kinetic parameters of the Pd loaded electrodes in 0.5 M H_2SO_4

Pd loading ($\mu\text{g}/\text{cm}^2$)	5	11	20	31	43	73	122
$E_{-10 \text{ mA/cm}^2}$ (mV)	-251	-171	-137	-123	-97	-84	-70
Tafel slope (mV/dec)	-146	-115	-90	-79	-69	-63	-53

The SEM micrographs (Figure 1a, b) reveal a uniform distribution of PdNPs across the entire graphite substrate. Figure 1a highlights the surface structure of the polycrystalline graphite, showcasing a rough nanoscale topography with a diverse array of features. These include flat, terrace-like regions alongside depressions and clefts, creating a

heterogeneous landscape that provides a variety of anchoring sites with distinct electronic properties. Despite this structural complexity, the even dispersion of PdNPs suggests that palladium growth seeds do not exhibit a preference for specific sites, enabling the formation of predominantly isolated nanoparticles. As shown in Figure 1b, analysis of the SEM image indicates that the individual particles reach a maximum size of approximately 90 nm at low Pd loading.

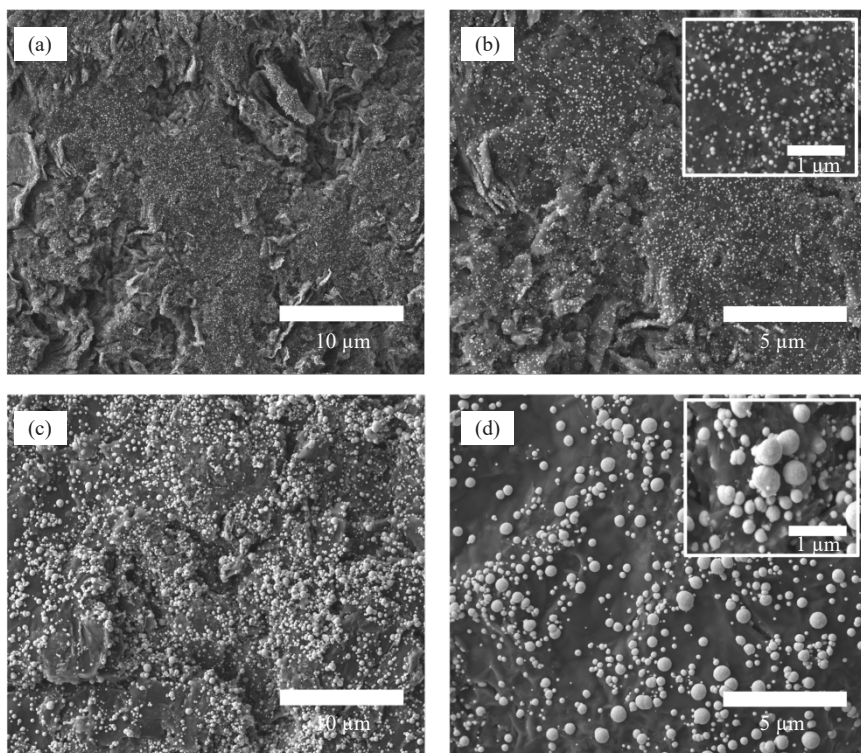


Figure 1. SEM micrographs of electrodeposited Pd nanoparticles on graphite: (a) Pd loading $m_{\text{pd}} = 21 \mu\text{g}/\text{cm}^2$, (c) Pd loading $m_{\text{pd}} = 119 \mu\text{g}/\text{cm}^2$; (b), (d) higher magnifications of (a) and (c)

In substrates with higher Pd loadings (Figure 1c), the nanoparticles remain well-distributed. Enlarged sections (Figure 1d) reveal primarily single particles, some as large as 520 nm, alongside occasional agglomerates formed by multiple nanoparticles merging. This combination of isolated particles and clusters indicates that increased deposition leads to both individual nanoparticle growth and localized aggregation.

The palladium nanoparticles display a rough surface texture, likely featuring multicrystalline facets that could favor hydrogen evolution reaction catalysis. Larger particles exhibiting pronounced polycrystallinity have been associated with an increased density of active sites characterized by lower hydrogen bonding energy [36]. These surface properties are particularly advantageous for palladium, which is known to lie on the strong hydrogen adsorption side of the volcano plot [37]. A reduction in the prevalence of high-strength Pd-H binding sites can improve hydrogen desorption kinetics, thereby enhancing catalytic performance. The nanoparticle morphologies observed in this study may therefore confer significant benefits for efficient hydrogen generation.

3.2 Catalytic HER performance

The electrocatalytic performance of palladium-decorated electrodes with varying metal loadings was evaluated through polarization curves, as illustrated in Figure 2a. These curves were corrected for solution resistance to accurately reflect the intrinsic activity of the electrode materials. The solution resistance, estimated at $0.8 \Omega \cdot \text{cm}^2$, was determined by measuring the high-frequency resistance (HFR) of a platinum plate under identical cell configurations [38]. This correction methodology ensures that the conductivity properties of the graphite substrates are not compensated, allowing

the electrocatalysis measurements to represent the electrode material's activity [39].

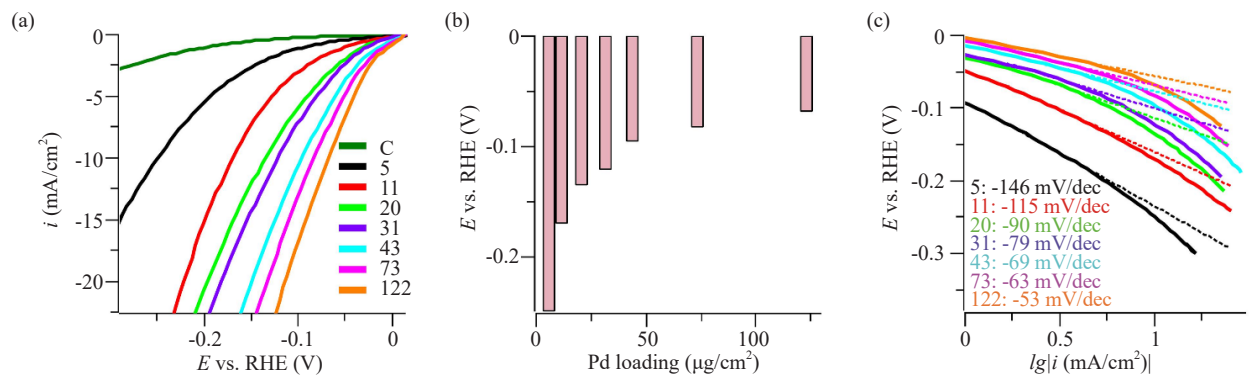


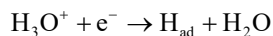
Figure 2. (a) Polarization curves of the palladium loaded electrodes ($5, 11, 20, 31, 43, 73, 122 \mu\text{g}/\text{cm}^2$ Pd); (b) overpotential at $-10 \text{ mA}/\text{cm}^2$ as a function of the Pd loading; (c) Tafel plots of the various electrodes

Analysis of the polarization curves reveals a clear trend of enhanced electrocatalytic activity correlating with increased palladium loading across all decorated electrodes. To quantitatively assess this relationship, the overpotentials required to achieve a current density of $-10 \text{ mA}/\text{cm}^2$ were determined for each electrode composition. These values, which reflect the performance of the hydrogen evolution catalysts, are summarized in Table 1.

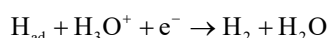
The investigated electrodes show a good capability to promote hydrogen evolution with rising Pd content. Already a very small Pd amount of $5 \mu\text{g}/\text{cm}^2$ reduces the overpotential by 169 mV compared to bare graphite which is essentially not HER catalytic. The highest Pd loaded graphite electrode needs only an overpotential of -70 mV for a current density of $-10 \text{ mA}/\text{cm}^2$. This activity is comparable to a commercial 20 wt% Pd/C electrode with an overpotential of approximately -76 mV [40].

The overpotential to drive a current of $-10 \text{ mA}/\text{cm}^2$ was observed to be strongly dependent on the amount of deposited palladium (Figure 2b). Already small amounts of Pd effect a significant reduction in the overpotential. However, this effect gradually flattens so that an increase in Pd from 73 to 122 $\mu\text{g}/\text{cm}^2$ results only in an overpotential reduction of 10 mV while an increase from 5 to 11 $\mu\text{g}/\text{cm}^2$ yield a reduction in overpotential of 80 mV. The notably smaller increase in Pd HER activity can be attributed to the formation of larger nanoparticles as the palladium loading increases. As evident from SEM micrographs, these larger particles exhibit a reduced surface area relative to their loading, in contrast to smaller nanoparticles. Furthermore, the tendency of nanoparticles to agglomerate limits the expansion of accessible surface area. As a result, the catalytic activity begins to flatten despite higher palladium loadings.

The analysis of Tafel plots with the logarithmic dependence of the current density i as a function of the overpotential E vs. RHE (Figure 2c) allows to gain insight into the kinetics and mechanism of HER. In acidic media, the formation of molecular hydrogen is a two-step process involving in the first step the discharge of the hydronium ion (H_3O^+) under the formation of a surface adsorbed hydrogen atom H_{ad} (Volmer step).



The formation of the hydrogen molecule can either proceed according to an electrochemical desorption reaction (Heyrovsky step).



or by recombination of two adsorbed hydrogen atoms (Tafel step).



The Tafel slope derived in a linear current density dependent overpotential region implies which mechanism is rate-determining. If the Volmer reaction is the rate-determining step of the hydrogen evolution, the Tafel slope should be about -120 mV/dec, while a rate determining Tafel or Heyrovsky mechanism should result in slopes of about -30 and -40 mV/dec, respectively [41, 42].

The Pd/C electrode with the highest loading ($122 \mu\text{g}/\text{cm}^2$) exhibits in the linear low overpotential region a Tafel slope of -53 mV/dec. This value is in the same range as the commercial 20 wt% Pd/C with -34 mV/dec [40]. The Tafel slope values indicate that the hydrogen evolution proceeds via the Volmer-Heyrovsky mechanism. This is characterized by a primary discharge step, followed by a slow electrochemical desorption reaction as the rate-determining step. In the high overpotential regime with current densities above $-10 \text{ mA}/\text{cm}^2$ the Tafel slopes increase due to the potential-dependent reaction rates of individual HER steps [43]. Due to the increased surface coverage of adsorbed hydrogen atoms at higher potentials, the Volmer discharge step is becoming rate-determining for the hydrogen formation [44].

The electrocatalytic performance of the PdNP-activated electrodes for the hydrogen evolution reaction aligns with previously reported results for various PdNP-decorated substrates. Notably, a study utilizing Pd nanoparticles on carbon black (CB) substrates demonstrated pronounced HER activity, achieving -53 mV at $-10 \text{ mA}/\text{cm}^2$ with a Tafel slope of -48.8 mV/dec for a 20.9 wt% Pd loading [45]. This superior performance was attributed to the hierarchical porosity of carbon black, which combines micro-, meso-, and macropores. Such a structure enhances nanoparticle dispersion and facilitates electrolyte penetration while reducing ion-transport resistance [46, 47].

The rough graphite substrate in this study exhibits an inhomogeneous surface morphology with diverse structural elements, akin to the hierarchical porosity of carbon black substrates. This unique topography provides numerous favorable Pd anchoring sites, ensuring highly accessible catalytically active areas. Similar to the benefits observed in carbon black, this configuration is believed to significantly contribute to the observed high HER activity by optimizing the electrode-electrolyte interface for efficient catalysis.

The identification of electrochemical desorption as the rate-determining step in hydrogen evolution aligns also with observations from composite systems such as Pd nanoparticles supported on MoS_2/CB ($0.14 \text{ mg Pd}/\text{cm}^2$) which displayed a Tafel slope of -57 mV/dec and an overpotential of -78 mV at $-10 \text{ mA}/\text{cm}^2$. Similarly, Pd/graphitic carbon nitride electrodes demonstrated values of -105 mV and -68 mV/dec [48]. These performance metrics, analogous to our findings, validate the efficacy of our catalyst design. The consistency across diverse support materials underscores the intrinsic catalytic properties of Pd nanoparticles for HER, highlighting their versatility in various electrocatalytic environments.

3.3 EIS studies

A deeper insight in HER kinetic processes can be obtained by electrochemical impedance spectroscopy. The impedance measurements were carried out with four electrodes with differing Pd loadings in the overpotential regime -10 mV to -65 mV vs. RHE.

Figure 3a-d show the Nyquist plots of electrodes loaded with 20, 43, 73 and $122 \mu\text{g}/\text{cm}^2$ Pd at selected overpotentials.

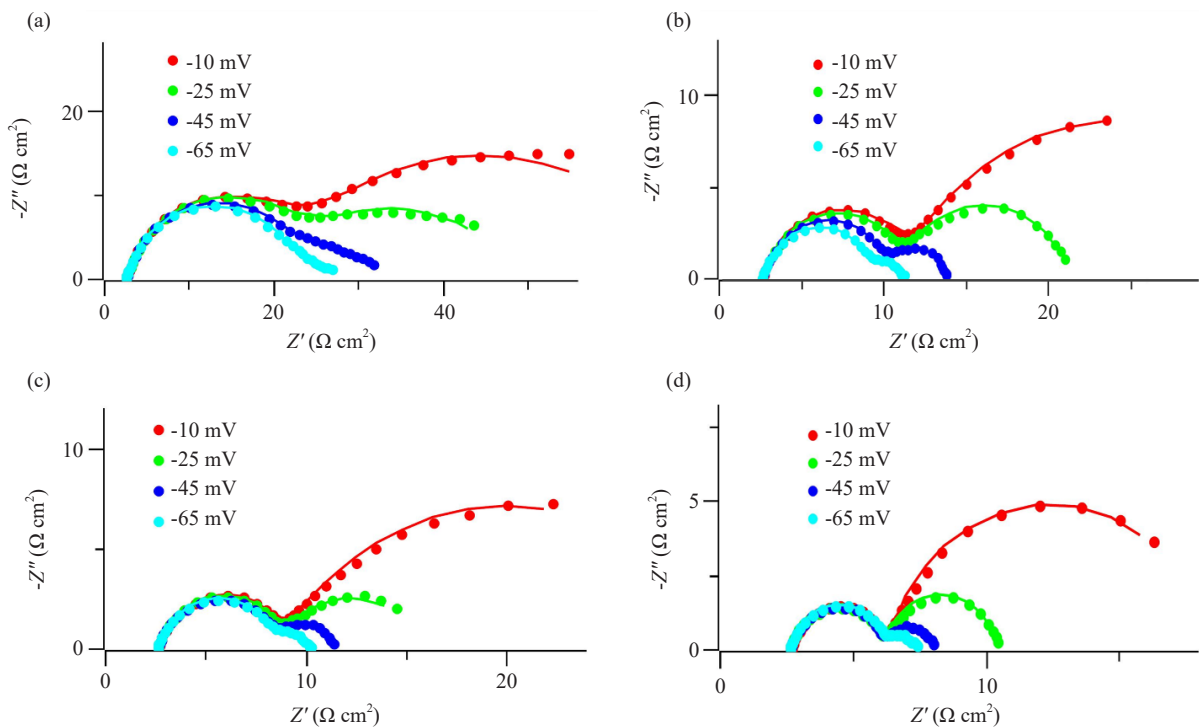


Figure 3. Nyquist plots at various overpotentials obtained for the Pd/C electrocatalysts with the Pd loadings (a) $20 \mu\text{g}/\text{cm}^2$, (b) $43 \mu\text{g}/\text{cm}^2$, (c) $73 \mu\text{g}/\text{cm}^2$, (d) $122 \mu\text{g}/\text{cm}^2$

In the investigated overpotential range, the complex plane plots of the nanoparticle-decorated substrates exhibit two overlapping semicircles at high and low frequencies, both slightly depressed towards the real axis. In electrochemical impedance spectroscopy, each semicircle typically corresponds to a distinct electrochemical process: the high-frequency semicircle is usually associated with charge transfer kinetics at the electrode-electrolyte interface, while the low-frequency semicircle often reflects slower processes such as hydrogen adsorption or mass transport limitations on the electrode surface [49, 50]. The relatively small size of the semicircles in the present measurements indicates low resistances for both charge and mass transfer, suggesting efficient electrode kinetics and minimal hindrance to these processes. This is a desirable feature, as it reflects the high catalytic activity and good accessibility of active sites on the Pd-decorated electrodes.

The dependence of the size of the semicircles with the cathodic overpotential further supports their kinetic origin [49, 51]. The clear separation between the semicircles—spanning approximately two orders of magnitude in timescale—allows these processes to be well resolved in the impedance spectra.

For the electrode with a Pd loading of $20 \mu\text{g}/\text{cm}^2$, a pronounced broadening and expansion of the low-frequency semicircle is observed. This effect indicates a distribution of relaxation times, which can be attributed to the high degree of surface heterogeneity, resulting in diverse hydrogen adsorption sites. Consequently, the impedance response at low frequencies extends over a wider range, leading to a flattened appearance of the curve in this region [52].

The shape of the EIS has been proposed to hint at possible tendencies in the electrocatalytic behavior of HER-active electrodes [53]. For high-activity Pt and Pd catalysts, two semicircles in the EIS, associated with distinct time constants and dependent on overpotential, may suggest a correlation with hydrogen binding energy near an optimal range for HER activity [54, 55].

The determination of the kinetic parameters from the EIS technique is performed by the fit of the experimental data to a model described by the two-time constant parallel equivalent circuit (Figure 4) [56, 32]. This model predicts the formation of two capacitive semicircles in the Nyquist plot which are related to the two time constants. Due to the deviation from ideal capacitive behavior which is manifested in the depressed shape of the capacitive response the constant phase elements CPE_1 and CPE_2 were introduced.

The impedance of the CPE is described by Equation 1

$$Z_{\text{CPE}} = \frac{1}{Q(j\omega)^n} \quad (1)$$

where Q is the capacitance parameter in $\text{F}\cdot\text{s}^{n-1}\cdot\text{cm}^{-2}$, j the imaginary unity, ω the angular frequency in rad/s and $n < 1$ dimensionless constant defining the deviation from ideal capacitive behavior with $n = 1$ [33]. The CPE accounts for electrode roughness and heterogeneity which produces a certain frequency dispersion leading to a flattening of the semicircle [57, 58]. By use of the constant phase elements sufficiently modelling of the impedimetric data is possible.

In Figure 4 the resistance R_s represents the electrolyte resistance measured between the working and reference electrode and is described by the intercept of the Nyquist plot with the real axis at the highest frequencies [33]. R_1 and CPE_1 are related to the reaction charge transfer kinetics, and R_2 and CPE_2 to mass transfer kinetics [55]. R_1 is the charge transfer resistance across the electrode/electrolyte interface, and CPE_1 is a constant phase element related to the double layer capacitance formed at the electrode/electrolyte interface. R_2 is a pseudo resistance and CPE_2 a constant phase element related to a pseudo capacitance [49].

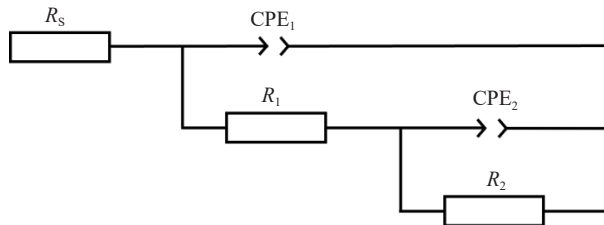


Figure 4. Equivalent electrical circuit with two parallel time constants used to model the EIS response of the HER

Figure 3a-d show that the equivalent circuit models properly the impedance response, manifesting a good agreement between experimental data (represented as symbols) and the fit. This indicates that the proposed model is suitable for the system under study.

The values for the electrochemical double-layer capacitance (C_{dl}) (Table 2) were determined from the equation proposed by Brug and collaborators that relates some of the parameters that make up the equivalent circuit of Figure 4 [59].

$$C_{\text{dl}} = \left[\frac{Q_1}{(R_s^{-1} + R_1^{-1})^{(1-n_1)}} \right]^{\frac{1}{n_1}} = Q_1^{\frac{1}{n_1}} (R_s^{-1} + R_1^{-1})^{1-\frac{1}{n_1}} \quad (2)$$

The values of the pseudocapacitance C_p were calculated from fit parameters of the equivalent circuit (Figure 4) using the modified Equation 2 according to [55].

$$C_p = Q_2^{\frac{1}{n_2}} \left[(R_s + R_1)^{-1} + R_2^{-1} \right]^{1-\frac{1}{n_2}} \quad (3)$$

Table 2 lists fitted EIS parameters and calculated capacitances C_{dl} and C_p obtained for the various decorated electrodes.

Table 2. Parameters obtained from the fitted impedance responses of Pd loaded graphite electrodes in 0.5 M H₂SO₄

Pd loading ($\mu\text{g}/\text{cm}^2$)	E vs. RHE (mV)	R_s ($\Omega \text{ cm}^2$)	R_1 ($\Omega \text{ cm}^2$)	R_2 ($\Omega \text{ cm}^2$)	C_{dl} (mF/cm^2)	C_p (mF/cm^2)
20	-10	2.69	22.2	38.2	0.54	20.9
	-25	2.69	21.8	23.9	0.53	27.6
	-45	2.69	20.5	8.92	0.50	43.3
	-65	2.68	19.9	4.27	0.47	78.0
43	-10	2.73	8.96	25.7	0.62	69.0
	-25	2.69	8.86	9.72	0.61	82.6
	-45	2.71	7.81	3.19	0.57	98.5
	-65	2.68	6.84	1.59	0.54	116
73	-10	2.73	6.27	22.9	0.98	168
	-25	2.71	6.26	7.02	0.96	161
	-45	2.70	6.11	2.62	0.89	152
	-65	2.69	5.96	1.59	0.83	137
122	-10	2.72	3.62	12.1	1.15	394
	-25	2.69	3.59	4.09	1.09	336
	-45	2.71	3.49	1.80	1.03	286
	-65	2.70	3.54	1.16	0.95	233

Table 2 indicates that both the double layer capacitance and the fitted charge transfer resistance decrease with increasing cathodic overpotential. This behavior, observed in the high-frequency semicircle of the impedance spectra, reflects the rapid charge transfer kinetics of the hydrogen evolution reaction. Here, C_{dl} represents the capacitance at the electrode-electrolyte interface, while R_1 corresponds to the resistance associated with HER charge transfer. Additionally, the coupled R_2-C_p behavior varies with cathodic overpotential and is accompanied by a reduction in the low-frequency semicircle. This response is attributed to hydrogen adsorption on the electrode surface, confirming that the low-frequency semicircle is linked to the pseudo-capacitance and resistance associated with the hydrogen adsorption phenomenon [60, 61].

As shown in Table 2, a common trend across all electrodes is the decrease in C_{dl} values with increasing HER overpotential. This can be attributed to a reduction in available active surface area due to hydrogen gas bubble formation at higher overpotentials, which blocks active sites and limits electrolyte access [62]. Conversely, changes in C_{dl} with Pd loading are attributed to an increase in active surface area, enhancing the catalytic performance.

Figure 5a illustrates the inverse relationship between charge transfer resistance and overpotential for various Pd loadings. A notable 10% reduction is observed when increasing the overpotential from -10 mV to -65 mV (20 $\mu\text{g}/\text{cm}^2$). This phenomenon stems from the enhanced driving force for the HER at higher cathodic biases, facilitating faster charge transfer kinetics and consequently accelerating the HER rate. The improved electron transfer capability manifests as a decrease in charge transfer resistance, coinciding with the contraction of the high-frequency semicircle in the Nyquist plot [63].

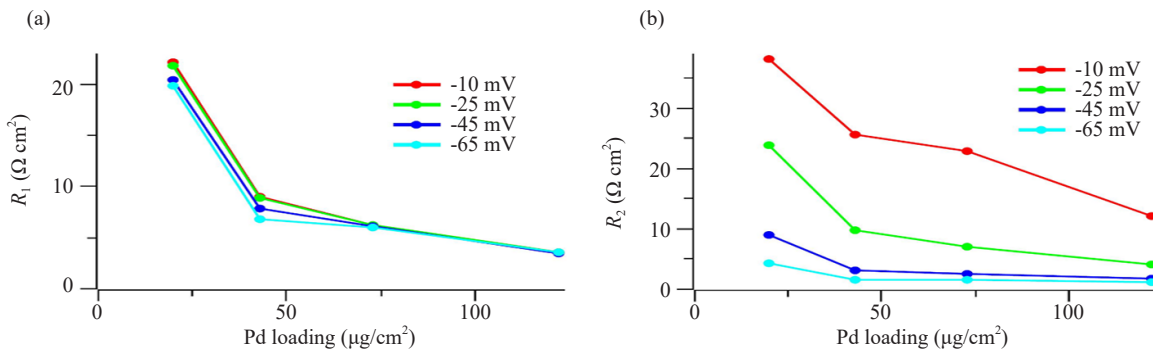


Figure 5. Resistance dependence on the Pd loading for different overpotentials (a) charge transfer resistance R_1 , (b) mass transfer resistance R_2

The impact of Pd loading on R_1 is considerably more pronounced. At -65 mV overpotential, R_1 diminishes by approximately 82% when increasing the catalyst amount from 20 to $122 \mu\text{g}/\text{cm}^2$. This substantial reduction, coupled with an expansion of the catalytically active surface area, indicates that Pd efficiently catalyzes the HER by promoting electron transfer to protons from the electrolyte [64]. Notably, a 65% decrease in R_1 is achieved by increasing the loading from 20 to $43 \mu\text{g}/\text{cm}^2$ (-65 mV). However, subsequent additions of Pd yield smaller returns. This observed behaviour can be attributed to the formation of larger nanoparticles and the onset of cluster aggregation at higher loadings potentially reducing the number of active sites available for catalysis relative to the total amount of Pd present. These structural modifications could explain why the enhancement in electrocatalytic performance does not directly correspond to the increment in Pd quantity.

Figure 5b illustrates a more rapid decrease in mass transfer resistance R_2 compared to R_1 as overpotential increases. Specifically, when the overpotential changes from -10 to -65 mV, R_2 experiences a substantial reduction of approximately 89% ($20 \mu\text{g}/\text{cm}^2$) or 90% ($122 \mu\text{g}/\text{cm}^2$), respectively. However, a flattening trend becomes apparent, indicating that further increases in overpotential yield progressively smaller decrements in R_2 , an effect that becomes more pronounced with higher Pd content. This phenomenon is also evident in the complex plane plot, where the low-frequency (LF) semicircle diminishes less and less in size with increasing overpotential.

The observed behavior can be attributed to a strong increase in surface coverage whereby in case of a constant surface coverage which is no more changing with overpotential the second semicircle may ultimately vanish [55]. This substantial rise in hydrogen coverage results in mass transport becoming less of a limiting factor for kinetics, while the electron transfer process increasingly dominates the impedance response at elevated overvoltages. This shift in dominance aligns with the observation of an increasingly rate-determining Volmer step at elevated overvoltages, suggesting that charge transfer kinetics become the primary governing factor of catalytic performance under these conditions. Consequently, a small charge transfer resistance facilitates enhanced catalytic activity towards hydrogen evolution. This finding is corroborated by electrochemical impedance spectroscopy studies on Pd-containing nanoparticle composite catalysts, which indicate that minimal charge transfer resistance promotes superior catalytic performance [63].

The impact of increasing palladium loading on electrochemical performance exhibits a nuanced relationship with overpotential. At the lowest overpotential, augmenting Pd content demonstrates the most pronounced effect, indicating that further increases in Pd loading still have the potential to enhance mass transfer kinetics. However, this relationship changes at higher overpotentials, where a Pd loading of $43 \mu\text{g}/\text{cm}^2$ yields a mass transfer resistance (R_2) that remains relatively constant despite additional increases in Pd content.

The experimental results indicate that for elevated overpotentials, a Pd loading of approximately $43 \mu\text{g}/\text{cm}^2$ is optimal, as it results in a low charge transfer resistance while mass transfer resistance (-65 mV) remains largely unchanged with further increases in loading. Additional palladium beyond this level does not significantly enhance either parameter, indicating that both charge transfer and mass transfer limitations are effectively addressed at $43 \mu\text{g}/\text{cm}^2$.

Corroborating evidence for this conclusion is provided by DC voltage investigations which demonstrate that the hydrogen evolution reaction is efficiently catalyzed when Pd loadings fall within this range.

This synergy between mass transfer optimization and charge transfer enhancement at a specific Pd loading suggests that such an optimized loading can lead to improved catalytic performance without necessitating excessive use of the precious metal, thereby potentially increasing both the efficiency and cost-effectiveness of Pd-based HER catalysts.

4. Conclusion

Graphite electrodes decorated with palladium nanoparticles were fabricated via constant current deposition onto pristine substrates. The hydrogen evolution reaction was efficiently catalyzed from a loading level of $43 \mu\text{g}/\text{cm}^2$. Beyond this threshold further increases in Pd content tended to have a diminishing effect on the catalytic efficiency.

Kinetic analyses corroborated the excellent electrocatalytic activity, evidenced by a Tafel slope of approximately $-53 \text{ mV}/\text{dec}$. EIS analysis revealed that at -65 mV overpotential, mass transfer limitations diminished, while charge transfer resistance became increasingly dominant as Pd content rose. Both resistive components exhibited their most pronounced decrease as the loading approached the critical value. These findings collectively demonstrate that even small quantities of Pd enable efficient HER electrocatalysis, with optimal performance achieved at moderate loadings.

Acknowledgement

The authors are grateful to Katharina Goetz for her support with the electrochemical measurements.

Conflict of interest

The corresponding author states that there is no conflict of interest. There was no specific funding for this project.

References

- [1] Wang Y, Chen KS, Mishler J, Cho SC, Adroher XC. A review of polymer electrolyte membrane fuel cells: Technology, applications, and needs on fundamental research. *Applied Energy*. 2011; 88(4): 981-1007. Available from: <https://doi.org/10.1016/j.apenergy.2010.09.030>.
- [2] Sharaf OZ, Orhan MF. An overview of fuel cell technology: Fundamentals and applications. *Renewable and Sustainable Energy Reviews*. 2014; 32: 810-853. Available from: <https://doi.org/10.1016/j.rser.2014.01.012>.
- [3] Guilbert D, Vitale G. Hydrogen as a clean and sustainable energy vector for global transition from fossil-based to zero-carbon. *Clean Technologies*. 2021; 3(4): 881-909. Available from: <https://doi.org/10.3390/cleantechnol3040051>.
- [4] Jiang R, Tung S, Tang Z, Li L, Ding L, Xi X, et al. A review of core-shell nanostructured electrocatalysts for oxygen reduction reaction. *Energy Storage Materials*. 2018; 12: 260-276. Available from: <https://doi.org/10.1016/j.ensm.2017.11.005>.
- [5] Cai J, Javed R, Ye D, Zhao H, Zhang J. Recent progress in noble metal nanocluster and single atom electrocatalysts for the hydrogen evolution reaction. *Journal of Materials Chemistry A*. 2020; 8(43): 22467-22487. Available from: <https://doi.org/10.1039/D0TA06942F>.
- [6] Kirubakaran A, Jain S, Nema RK. A review on fuel cell technologies and power electronic interface. *Renewable and Sustainable Energy Reviews*. 2009; 13(9): 2430-2440. Available from: <https://doi.org/10.1016/j.rser.2009.04.004>.
- [7] Abdin Z, Zafaranloo A, Rafiee A, Mérida W, Lipiński W, Khalilpour KR. Hydrogen as an energy vector. *Renewable and Sustainable Energy Reviews*. 2020; 120: 109620. Available from: <https://doi.org/10.1016/j.rser.2019.109620>.
- [8] Luo F, Guo L, Xie Y, Xu J, Qu K, Yang Z. Iridium nanorods as a robust and stable bifunctional electrocatalyst for pH-universal water splitting. *Applied Catalysis B: Environmental*. 2020; 279: 119394. Available from: <https://doi.org/10.1016/j.apcatb.2020.119394>.
- [9] Xiu L, Pei W, Zhou S, Wang Z, Yang P, Zhao J, et al. Multilevel hollow MXene tailored low-Pt catalyst for efficient hydrogen evolution in full-pH range and seawater. *Advanced Functional Materials*. 2020; 30(47): 1910028.

- Available from: <https://doi.org/10.1002/adfm.201910028>.
- [10] Harichandan S, Kar SK, Rai PK. A systematic and critical review of green hydrogen economy in India. *International Journal of Hydrogen Energy*. 2023; 48(81): 31425-31442. Available from: <https://doi.org/10.1016/j.ijhydene.2023.04.316>.
 - [11] Whitehead J, Newman P, Whitehead J, Lim KL. Striking the right balance: Understanding the strategic applications of hydrogen in transitioning to a net zero emissions economy. *Sustainable Earth Reviews*. 2023; 6(1): 1-10. Available from: <https://doi.org/10.1186/s42055-022-00049-w>.
 - [12] Jiao Y, Zheng Y, Jaroniec M, Qiao SZ. Design of electrocatalysts for oxygen-and hydrogen-involving energy conversion reactions. *Chemical Society Reviews*. 2015; 44(8): 2060-2086. Available from: <https://doi.org/10.1039/C4CS00470A>.
 - [13] Faber MS, Jin S. Earth-abundant inorganic electrocatalysts and their nanostructures for energy conversion applications. *Energy & Environmental Science*. 2014; 7(11): 3519-3542. Available from: <https://doi.org/10.1039/C4EE01760A>.
 - [14] Song J, Wei C, Huang ZF, Liu C, Zeng L, Wang X, et al. A review on fundamentals for designing oxygen evolution electrocatalysts. *Chemical Society Reviews*. 2020; 49(7): 2196-2214. Available from: <https://doi.org/10.1039/C9CS00607A>.
 - [15] Hu C, Zhang L, Gong J. Recent progress made in the mechanism comprehension and design of electrocatalysts for alkaline water splitting. *Energy and Environmental Science*. 2019; 12(9): 2620-2645. Available from: <https://doi.org/10.1039/C9EE01202H>.
 - [16] Liu HL, Nosheen F, Wang X. Noble metal alloy complex nanostructures: Controllable synthesis and their electrochemical property. *Chemical Society Reviews*. 2015; 44(10): 3056-3078. Available from: <https://doi.org/10.1039/C4CS00478G>.
 - [17] Liu J, Ma Q, Huang Z, Liu G, Zhang H. Recent progress in graphene-based noble-metal nanocomposites for electrocatalytic applications. *Advanced Materials*. 2019; 31(9): 1800696. Available from: <https://doi.org/10.1002/adma.201800696>.
 - [18] Yang F, Xiong T, Huang P, Zhou S, Tan Q, Yang H, et al. Nanostructured transition metal compounds coated 3D porous core-shell carbon fiber as monolith water splitting electrocatalysts: A general strategy. *Chemical Engineering Journal*. 2021; 423: 130279. Available from: <https://doi.org/10.1016/j.cej.2021.130279>.
 - [19] Huang H, Jung H, Park CY, Kim S, Lee A, Jun H, et al. Surface conversion derived core-shell nanostructures of Co particles@RuCo alloy for superior hydrogen evolution in alkali and seawater. *Applied Catalysis B: Environmental*. 2022; 315: 121554. Available from: <https://doi.org/10.1016/j.apcatb.2022.121554>.
 - [20] Liu L, Corma A. Metal catalysts for heterogeneous catalysis: From single atoms to nanoclusters and nanoparticles. *Chemical Reviews*. 2018; 118(10): 4981-5079. Available from: <https://doi.org/10.1021/acs.chemrev.7b00776>.
 - [21] Cheng N, Stambula S, Wang D, Banis MN, Liu J, Riese A, et al. Platinum single-atom and cluster catalysis of the hydrogen evolution reaction. *Nature Communications*. 2016; 7(1): 13638. Available from: <https://doi.org/10.1038/ncomms13638>.
 - [22] Huang X, Zeng Z, Bao S, Wang M, Qi X, Fan Z, et al. Solution-phase epitaxial growth of noble metal nanostructures on dispersible single-layer molybdenum disulfide nanosheets. *Nature Communications*. 2013; 4(1): 1444. Available from: <https://doi.org/10.1038/ncomms2472>.
 - [23] Antolini E. Palladium in fuel cell catalysis. *Energy & Environmental Science*. 2019; 2(9): 915-931. Available from: <https://doi.org/10.1039/B820837A>.
 - [24] Shao M. Palladium-based electrocatalysts for hydrogen oxidation and oxygen reduction reactions. *Journal of Power Sources*. 2011; 196(5): 2433-2444. Available from: <https://doi.org/10.1016/j.jpowsour.2010.10.093>.
 - [25] Chang J, Feng L, Liu C, Xing W, Hu X. Ni₂P enhances the activity and durability of the Pt anode catalyst in direct methanol fuel cells. *Energy and Environmental Science*. 2014; 7(5): 1628-1632. Available from: <https://doi.org/10.1039/C4EE00100A>.
 - [26] Liu M, Zhang R, Chen W. Graphene-supported nanoelectrocatalysts for fuel cells: Synthesis, properties, and applications. *Chemical Reviews*. 2014; 114(10): 5117-5160. Available from: <https://doi.org/10.1021/cr400523y>.
 - [27] Guo S, Dong S, Wang E. Constructing carbon nanotube/Pt nanoparticle hybrids using an imidazolium-salt-based ionic liquid as a linker. *Advanced Materials*. 2010; 22(11): 1269-1272. Available from: <https://doi.org/10.1002/adma.200903379>.
 - [28] Bessel CA, Laubernds K, Rodriguez NM, Baker RTK. Graphite nanofibers as an electrode for fuel cell applications. *The Journal of Physical Chemistry B*. 2001; 105(6): 1115-1118. Available from: <https://doi.org/10.1021/jp003280d>.
 - [29] Huang H, Yan M, Yang C, He H, Jiang Q, Yang L, et al. Graphene nanoarchitectonics: Recent advances in

- graphene-based electrocatalysts for hydrogen evolution reaction. *Advanced Materials*. 2019; 31(48): 1903415. Available from: <https://doi.org/10.1002/adma.201903415>.
- [30] Hao J, Wei F, Zhang X, Li L, Zhang C, Liang D, et al. Defect and doping engineered penta-graphene for catalysis of hydrogen evolution reaction. *Nanoscale Research Letters*. 2021; 16: 1-9. Available from: <https://doi.org/10.1186/s11671-021-03590-3>.
- [31] Zhang H, Noonan O, Huang X, Yang Y, Xu C, Zhou L, et al. Surfactant-free assembly of mesoporous carbon hollow spheres with large tunable pore sizes. *ACS Nano*. 2016; 10(4): 4579-4586. Available from: <https://doi.org/10.1021/acsnano.6b00723>.
- [32] Lasia A. *Electrochemical Impedance Spectroscopy and its Applications*. New York: Springer; 2014.
- [33] Lazanas AC, Prodromidis MI. Electrochemical Impedance Spectroscopy—A Tutorial. *ACS Measurements Science Au*. 2023; 3(3): 162-193. Available from: <https://doi.org/10.1021/acsmeasuresciau.2c00070>.
- [34] Hansen JN, Prats H, Toudahl KK, Mørch Secher N, Chan K, Kibsgaard J, et al. Is there anything better than Pt for HER? *ACS Energy Letters*. 2021; 6(4): 1175-1180. Available from: <https://doi.org/10.1021/acsenergylett.1c00246>.
- [35] Gulumian M, Andraos C, Afantitis A, Pubyn T, Coville NJ. Importance of surface topography in both biological activity and catalysis of nanomaterials: Can catalysis by design guide safe by design? *International Journal of Molecular Sciences*. 2021; 22(15): 8347. Available from: <https://doi.org/10.3390/ijms22158347>.
- [36] Zheng J, Zhou S, Gu S, Xu B, Yan Y. Size-dependent hydrogen oxidation and evolution activities on supported palladium nanoparticles in acid and base. *Journal of the Electrochemical Society*. 2016; 163(6): F499-F506. Available from: <https://doi.org/10.1149/2.0661606jes>.
- [37] Zheng Y, Jiao Y, Zhu Y, Li LH, Han Y, Chen Y, et al. Hydrogen evolution by a metal-free electrocatalyst. *Nature Communications*. 2014; 5(1): 3783. Available from: <https://doi.org/10.1038/ncomms4783>.
- [38] Zheng W. IR compensation for electrocatalysis studies: Considerations and recommendations. *ACS Energy Letters*. 2023; 8(4): 1952-1958. Available from: <https://doi.org/10.1021/acsenergylett.3c00366>.
- [39] Chung DY, Park S, Lopes PP, Stamenkovic VR, Sung YE, Markovic NM, et al. Electrokinetic analysis of poorly conductive electrocatalytic materials. *ACS Catalysis*. 2020; 10(9): 4990-4996. Available from: <https://doi.org/10.1021/acscatal.0c00960>.
- [40] Aygün M, Guillen-Soler M, Vila-Fungueirín JM, Kurtoglu A, Chamberlain TW, Khlobystov AN, et al. Palladium nanoparticles hardwired in carbon nanoreactors enable continually increasing electrocatalytic activity during the hydrogen evolution reaction. *ChemSusChem*. 2021; 14(22): 4973-4984. Available from: <https://doi.org/10.1002/cssc.202101236>.
- [41] Conway BE, Tilak BV. Interfacial processes involving electrocatalytic evolution and oxidation of H₂, and the role of chemisorbed H. *Electrochimica Acta*. 2002; 47(22-23): 3571-3594. Available from: [https://doi.org/10.1016/S0013-4686\(02\)00329-8](https://doi.org/10.1016/S0013-4686(02)00329-8).
- [42] Pentland N, Bockris JO'M, Sheldon E. Hydrogen evolution reaction on copper, gold, molybdenum, palladium, rhodium, and iron: Mechanism and measurement technique under high purity conditions. *Journal of The Electrochemical Society*. 1957; 104(3): 182. Available from: <https://doi.org/10.1149/1.2428530>.
- [43] Lasia A. Mechanism and kinetics of the hydrogen evolution reaction. *International Journal of Hydrogen Energy*. 2019; 44(36): 19484-19518. Available from: <https://doi.org/10.1016/j.ijhydene.2019.05.183>.
- [44] Shinagawa T, Garcia-Esparza AT, Takanabe K. Insight on Tafel slopes from a microkinetic analysis of aqueous electrocatalysis for energy conversion. *Scientific Reports*. 2015; 5(1): 13801. Available from: <https://doi.org/10.1038/srep13801>.
- [45] Chantaramethakul J, Hussakan C, Yenmankhong Y, Chandeang P, Techapiesancharoenkij R, Hirunpinyopas W, et al. Effect of carbon black supports on the hydrogen evolution reaction activity of Pd nanoparticle electrocatalysts synthesized via solution plasma sputtering. *RSC Advances*. 2024; 14(43): 31648-31654. Available from: <https://doi.org/10.1039/D4RA04809A>.
- [46] Yan X, Li H, Sun J, Liu P, Zhang H, Xu B, et al. Pt nanoparticles decorated high-defective graphene nanospheres as highly efficient catalysts for the hydrogen evolution reaction. *Carbon*. 2018; 137: 405-410. Available from: <https://doi.org/10.1016/j.carbon.2018.05.046>.
- [47] Yu Y, Liu P, Dou M, Niu J, Zhang Z, Wang F. Promotion of hydrogen evolution catalysis by ordered hierarchically porous electrodes. *Catalysis Science & Technology*. 2021; 11(9): 2997-3001. Available from: <https://doi.org/10.1039/D1CY00401H>.
- [48] Woldetinsay M, Soreta TR, Maiyalagan T, Femi OE. Effect of support material on the electrocatalytic activity of palladium nanoparticle toward hydrogen evolution reaction. *Materials Research Express*. 2021; 8(2): 025501. Available from: <https://doi.org/10.1088/2053-1591/abdf1c>.

- [49] Medina-Orta R, Ortega EM, Pérez-Herranz V, Sánchez-Loredo MG. Nanostructured Pd/Ag/Ni electrocatalysts for the hydrogen evolution reaction. *Materials Today Communications*. 2024; 38: 108354. Available from: <https://doi.org/10.1016/j.mtcomm.2024.108354>.
- [50] Koster D, Zeradjanin AR, Battistel A, La Mantia F. Extracting the kinetic parameters of the hydrogen evolution reaction at Pt in acidic media by means of dynamic multi-frequency analysis. *Electrochimica Acta*. 2019; 308: 328-336. Available from: <https://doi.org/10.1016/j.electacta.2019.04.013>.
- [51] Birry L, Lasia A. Studies of the hydrogen evolution reaction on raney nickel-molybdenum electrodes. *Journal of Applied Electrochemistry*. 2004; 34: 735-749. Available from: <https://doi.org/10.1023/B:JACH.0000031161.26544.6a>.
- [52] Kumar S, Kumar R, Goyal N, Yadav A, BM S, Sahoo B. Nickel-embedded carbon nanostructures as noble metal-free catalysts for the hydrogen evolution reaction. *ACS Applied Nano Materials*. 2024; 7(14): 16422-16437. Available from: <https://doi.org/10.1021/acsanm.4c02278>.
- [53] Huang J. Correlation between electrocatalytic activity and impedance shape: A theoretical analysis. *PRX Energy*. 2024; 3(2): 023001. Available from: <https://doi.org/10.1103/PRXEnergy.3.023001>.
- [54] Barber JH, Conway BE. Structural specificity of the kinetics of the hydrogen evolution reaction on the low-index surfaces of Pt single-crystal electrodes in 0.5 M dm⁻³ NaOH. *Journal of Electroanalytical Chemistry*. 1999; 461(1-2): 80-89. Available from: [https://doi.org/10.1016/S0022-0728\(98\)00161-2](https://doi.org/10.1016/S0022-0728(98)00161-2).
- [55] Lin D, Lasia A. Electrochemical impedance study of the kinetics of hydrogen evolution at a rough palladium electrode in acidic solution. *Journal of Electroanalytical Chemistry*. 2017; 785: 190-195. Available from: <http://dx.doi.org/10.1016/j.jelechem.2016.12.037>.
- [56] Rakočević L, Golubović J, Latas N, Popović A, Rajić V, Štrbac S. Hydrogen evolution on Ir nanoparticles supported by glassy carbon and graphene nanoplatelets. *Journal of Electroanalytical Chemistry*. 2025; 977: 118871. Available from: <https://doi.org/10.1016/j.jelechem.2024.118871>.
- [57] Lasia A. The origin of the constant phase element. *Journal of Physical Chemistry Letters*. 2022; 13: 580-589. Available from: <https://doi.org/10.1021/acs.jpclett.1c03782>.
- [58] Gateman SM, Gharbi O, Gomes de Melo H, Ngo K, Turmine M, Vivier V. On the use of a constant phase element (CPE) in electrochemistry. *Current Opinion in Electrochemistry*. 2022; 36: 101133. Available from: <https://doi.org/10.1016/j.coelec.2022.101133>.
- [59] Brug GJ, van den Eeden ALG, Sluyters-Rehbach M, Sluyters JH. The analysis of electrode impedances complicated by the presence of a constant phase element. *Journal of Electroanalytical Chemistry*. 1984; 176: 275-295. Available from: [https://doi.org/10.1016/S0022-0728\(84\)80324-1](https://doi.org/10.1016/S0022-0728(84)80324-1).
- [60] Navarro-Flores E, Chong Z, Omanovic S. Characterization of Ni, NiMo, NiW and NiFe electroactive coatings as electrocatalysts for hydrogen evolution in an acidic medium. *Journal of Molecular Catalysis*. 2005; 226: 179-197. Available from: <https://doi.org/10.1016/j.molcata.2004.10.029>.
- [61] Herraiz-Cardona I, Ortega E, Pérez-Herranz VJE. Impedance study of hydrogen evolution on Ni/Zn and Ni-Co/Zn stainless steel based electrodeposits. *Electrochimica Acta*. 2011; 56(3): 1308-1315. Available from: <https://doi.org/10.1016/j.electacta.2010.10.093>.
- [62] Pierozynski B, Smoczynski L. Kinetics of hydrogen evolution reaction at nickel-coated carbon fiber materials in 0.5 M H₂SO₄ and 0.1 M NaOH solutions. *Journal of the Electrochemical Society*. 2009; 156(9): B1045-B1050. Available from: <https://doi.org/10.1149/1.3158518>.
- [63] Pitchai C, Vedanarayanan M, Gopalakrishnan SM. Efficient hydrogen evolution electrocatalysis using nitrogen doped carbon dot decorated palladium copper nanocomposites in acid medium. *New Journal of Chemistry*. 2023; 47(30): 14355-14363. Available from: <https://doi.org/10.1039/D3NJ01631E>.
- [64] Zeng Z, Küspert S, Balaghi SE, Hussein HE, Ortlieb N, Knäbbeler-Buß M, et al. Ultrahigh mass activity Pt entities consisting of Pt single atoms, clusters, and nanoparticles for improved hydrogen evolution reaction. *Small*. 2023; 19(29): 2205885. Available from: <https://doi.org/10.1002/smll.202205885>.